The influence of nanoscale phase separation and devitrification on the electrical transport properties of amorphous Cu–Nb alloy thin films

2009 J. Phys.: Condens. Matter 21 285305

(http://iopscience.iop.org/0953-8984/21/28/285305)

IOP Publishing Journal of Physics: Condensed Matter

J. Phys.: Condens. Matter **21** (2009) 285305 (5pp) doi:10.1088/0953-8984/21/28/285305

The influence of nanoscale phase separation and devitrification on the electrical transport properties of amorphous Cu–Nb alloy thin films

Sangita Bose[1,3], **Anantha Puthucode**[2], **Rajarshi Banerjee**[2] and **Pushan Ayyub**[1]

[1] Department of Condensed Matter Physics and Materials Science, Tata Institute of Fundamental Research, Mumbai 400005, India

[2] Department of Materials Science and Engineering, University of North Texas, Denton, TX 76203-5310, USA

Received 10 March 2009, in final form 16 May 2009

Published 19 June 2009

Online at stacks.iop.org/JPhysCM/21/285305

Abstract

The formation of amorphous phases in immiscible alloys with a large positive enthalpy of mixing is thermodynamically unfavorable. Co-sputter deposited Cu–Nb films exhibit a nanoscale phase separation into Cu-rich and Nb-rich amorphous regions. They show relatively high room temperature resistivity, a negative temperature coefficient of resistance (TCR), and an incomplete superconducting transition with onset at 3.7 K. Annealing the nanophase-separated amorphous films at 200 °C results in the nucleation of fcc Cu-rich nanocrystals within an Nb-rich amorphous matrix. This film exhibits multiple resistance steps, eventually showing a sharp drop with $(T_C)_{onset} = 3.7$ K. Annealing at 350 °C leads to complete devitrification via the formation of large bcc Nb-rich grains encapsulating the existing fcc Cu nanocrystals. These films show low room temperature resistivity, positive TCR, and a sharp superconducting transition with onset at 5.2 K. The electrical transport and superconducting behavior appear to be consistent with a two-stage crystallization process.

1. Introduction

The constituents of most classic glass-forming systems typically exhibit a large negative enthalpy of mixing, especially in the liquid phase [1]. The formation of amorphous phases in immiscible systems with a large *positive* enthalpy of mixing in the liquid phase is therefore rather unexpected. However, there are several instances of immiscible systems forming amorphous phases, such as: Ag–Ni [2, 3], Cu–Nb [4, 5], Ag–Cu [6, 7], Ag–Fe [8], Ag–Gd [9], Cu–Ta [10], and Cu–W [10]. Based on x-ray absorption fine structure studies coupled with atomistic simulations, He *et al* [2, 3] attributed the stabilization of amorphous phases in the immiscible Ag–Ni system to nanoscale phase separation, More recently, using three-dimensional atom probe (3DAP) tomography, we have shown direct evidence for nanoscale phase separation leading to the formation of 2–3 nm Cu-rich and Nb-rich clusters in sputter deposited, amorphous Cu–Nb alloy thin films [11]. Such nanoscale phase separation is expected to reduce the enthalpy (and consequently the free energy) in these far-from equilibrium, immiscible alloys. The nature of the variation of the microstructure over the entire composition range (from 5 to 90 at.% Nb) in the Cu–Nb system was reported later [12]. Samples in the composition range 25–65 at.% Nb are found to be completely amorphous. In this paper we focus on the unusual thermal evolution of the novel, nanoscale phase-separated microstructure of one of the 'amorphous' samples with the specific composition Cu–45 at.%Nb. We show that the electrical transport behavior in the as-deposited and sequentially annealed samples can be understood, at least qualitatively, on the basis of their microstructural evolution.

[3] Present address: Max Planck Institute for Solid State Research, Heisenbergstrasse 1, D-70569 Stuttgart, Germany.

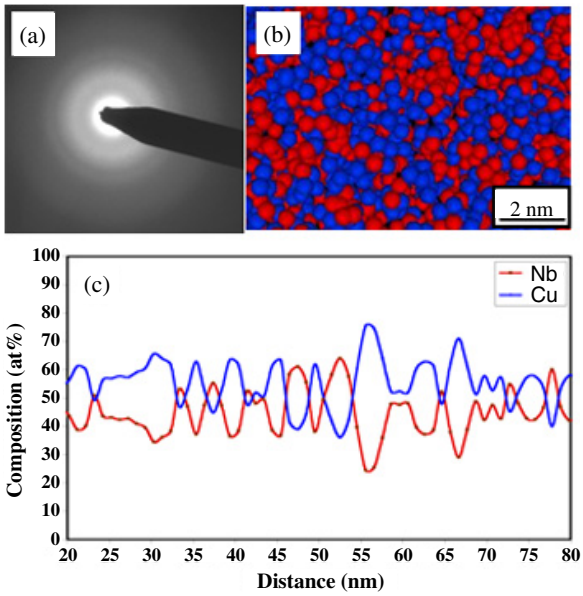

Figure 1. (a) Electron diffraction pattern and (b) 3D atom probe (3DAP) tomographic image showing the distribution of the Cu (blue) and Nb (red) atoms in the as-deposited, amorphous Cu–Nb alloy thin films. (c) Compositional profile along a 60 nm length, averaged over a cylinder of diameter 2 nm, obtained from the 3DAP reconstruction for the same sample, showing nanoscale clustering of Cu-rich and Nb-rich regions.

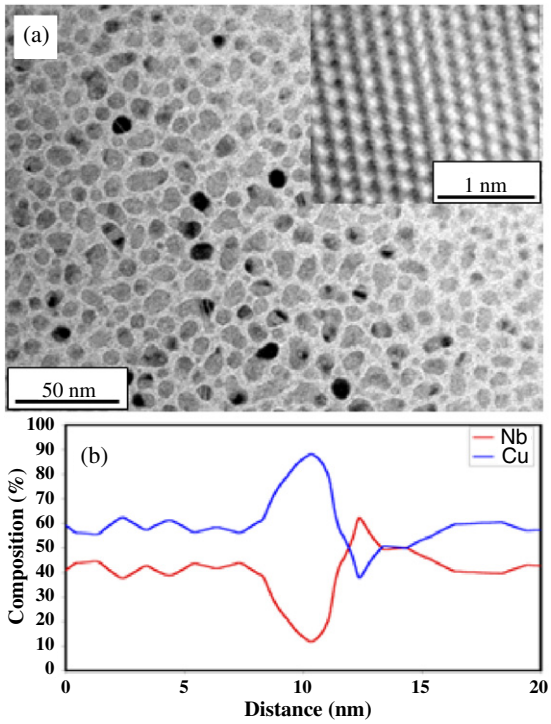

Figure 2. (a) A bright-field TEM image from the Cu–Nb film annealed at 200 °C for 3 h, showing fcc nanocrystals. The inset shows a high-resolution TEM image from one such fcc nanocrystal. (b) Compositional profile (3DAP) along a length of 60 nm, averaged over a cylinder of diameter 2 nm, across one of the fcc nanocrystals of the same sample.

2. Experimental details

The Cu–Nb alloy thin films were deposited by dc magnetron co-sputtering from pure elemental Cu (99.99%) and Nb (99.99%) targets obtained from Kurt Lesker Co. The base pressure was 1×10^{-7} Torr and the Ar gas pressure maintained during sputtering was 5×10^{-3} Torr. Films with a nominal composition of Cu–45 at.%Nb and thickness of 2–3 μm were deposited on Si(100) wafers. For the 3DAP studies, films were deposited under conditions identical to the above on a 6×6 array of flat-top silicon microtips. Further details about the sample preparation have been discussed elsewhere [11]. The as-deposited films were subsequently vacuum annealed (under 1×10^{-7} Torr) at different temperatures. The microstructure of the films was studied by a FEI Tecnai F20 FEG-TEM (field emission transmission electron microscope) operating at 200 kV, and by 3DAP tomography using an Imago LEAP™ system in the electric-field evaporation mode at 70 K, with an evaporation rate of ∼0.2% and a pulsing voltage at 30% of the steady-state voltage. Electrical resistivity measurements were performed using the standard four-probe geometry in a temperature controlled liquid He dewar.

3. Results

3.1. Microstructure

The electron diffraction pattern from the as-deposited film (figure 1(a)) confirms its amorphous nature. Figure 1(b) shows the distribution of individual Cu (blue) and Nb (red) atoms within the amorphous phase obtained from 3DAP tomography, while figure 1(c) shows the compositional profile averaged over a cylinder of length ∼60 nm and diameter 2 nm, also obtained from a 3DAP reconstruction. Clearly, the as-deposited film exhibits nanoscale phase separation leading to an intermixture of two distinct amorphous regions, one Cu-rich and the other Nb-rich, each with a characteristic size of ∼2–3 nm. The *average* compositions of the Cu-rich and Nb-rich regions are Cu–30 at.%Nb and Cu–60 at.%Nb, respectively. Further details about the structure and chemistry of the as-deposited amorphous Cu–Nb alloy are discussed in [11].

Annealing the amorphous bi-phasic films even at relatively low temperatures leads to distinct and interesting microstructural changes related to devitrification. A bright-field TEM image from the Cu–Nb film annealed at 200 °C for 3 h (figure 2(a)) shows fcc nanocrystals in the 5–10 nm size range, uniformly distributed within an amorphous matrix [13]. The inset shows a high-resolution TEM image from within one of the nanocrystals (with a twin defect), corresponding to the ⟨011⟩ axis of the fcc crystal. The composition of the nanocrystalline phase was identified by 3DAP tomography. A 3DAP compositional profile averaged over a cylinder of 2 nm diameter, across one of the fcc nanocrystals (see figure 2(b)) shows it to be a Cu-rich phase. The maximum Cu concentration observed is ∼90 at.% near the center of the nanocrystal, while the average composition of this phase is ∼Cu–20 at.%Nb.

Annealing the Cu–Nb films at 350 °C for 3 h resulted in the nucleation of large grains of a bcc Nb-rich phase,

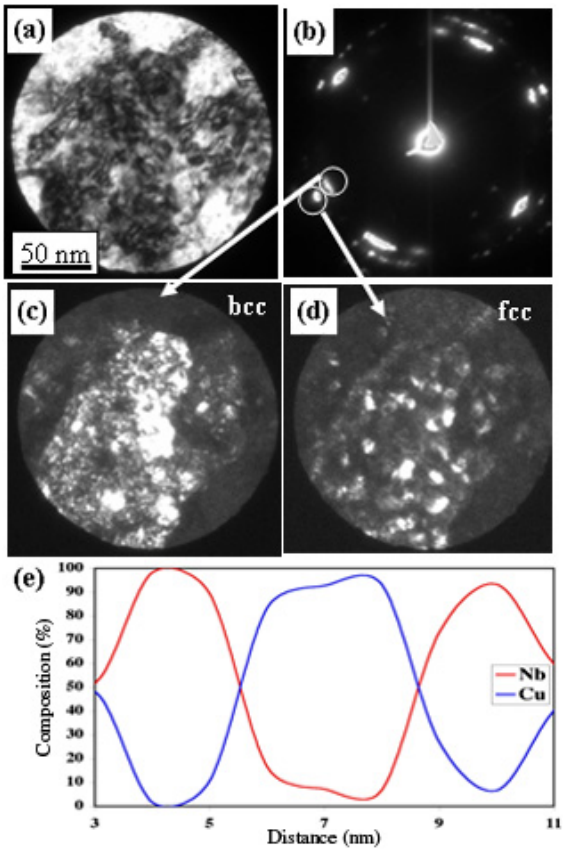

Figure 3. (a) Bright-field TEM image and (b) electron diffraction pattern of a bcc Nb-rich crystal in the Cu–Nb film annealed at 350 °C for 3 h. Dark-field TEM images of the same sample, recorded from reflections arising from the bcc Nb-rich phase and the fcc Cu-rich phase, are shown in (c) and (d), respectively. (e) A 3DAP compositional profile across an fcc Cu-rich nanocrystal embedded within a bcc Nb-rich grain in the same sample.

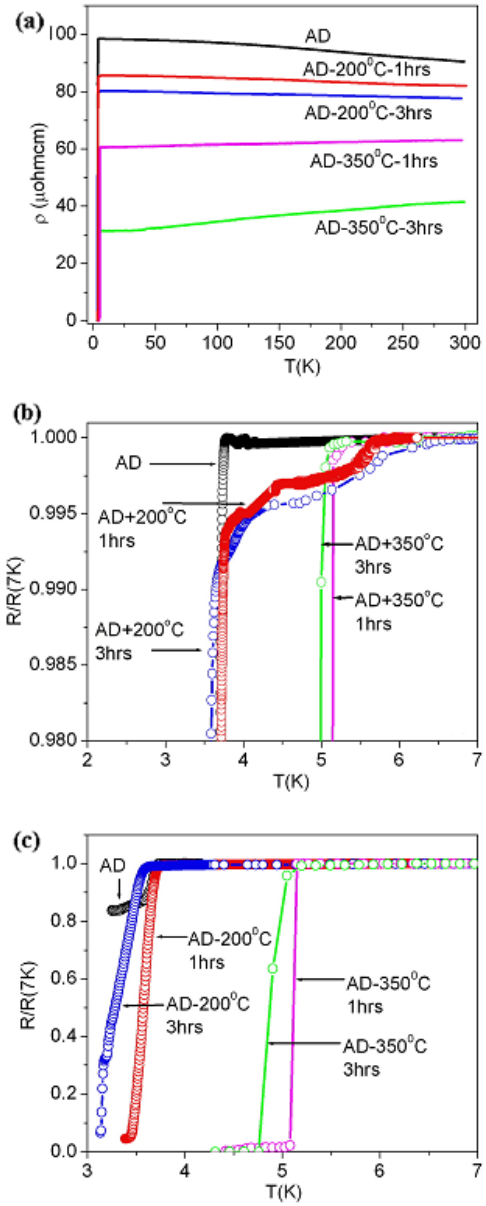

Figure 4. (a) shows the temperature dependence of the resistivity of (i) as-deposited (AD) Cu–Nb film, and after annealing at (ii) 200 °C for 1 h, (iii) 200 °C for 3 h, (iv) 350 °C for 1 h, and (v) 350 °C for 3 h. (b) and (c) show the normalized resistance of the same films at low temperature, providing details of the onset of the superconducting transition (b) and the zero-resistance region (c), respectively.

quite distinct from the pre-existing fcc Cu-rich nanocrystals. Figure 3(a) shows the bright-field image of one such bcc crystal. The corresponding electron diffraction pattern (figure 3(b)) contains reflections from the ⟨111⟩ zone axis of the bcc Nb-rich phase, as well as those from the ⟨011⟩ zone axis of the fcc Cu-rich phase, indicating that these grains consist of *both* phases. Dark-field images, recorded from specific reflections of the bcc and fcc phases, are shown in figures 3(c) and (d) respectively. These two dark-field images clearly indicate that this sample essentially consists of many small (∼10 nm) fcc Cu-rich crystallites embedded within each of the larger (∼100 nm) bcc Nb-rich crystallites. A 3DAP compositional profile across an fcc Cu-rich nanocrystal embedded within a bcc Nb-rich grain is shown in figure 3(e). The average fcc phase composition is ∼Cu–5 at.%Nb while that of the bcc phase is ∼Cu–95 at.% Nb, with some regions exhibiting close to pure elemental compositions.

3.2. Electrical transport

Figure 4(a) shows the temperature dependence of the electrical resistivity (ρ)—in the temperature range 3–300 K—of the as-deposited (AD) Cu–Nb thin film and of those after annealing at 200 and 350 °C for different times. For the AD sample and those annealed at 200 °C, the ρ–T plots exhibit a negative temperature coefficient of resistance (TCR). The room temperature resistivity ($\rho_{300\ \mathrm{K}}$) decreases from ∼90 $\mu\Omega$ cm for the AD film to ∼78 $\mu\Omega$ cm for that annealed at 200 °C for 3 h. The Cu–Nb films annealed at 350 °C are completely devitrified and exhibit a positive TCR, with further lowering of $\rho_{300\ \mathrm{K}}$ to 63 $\mu\Omega$ cm (350 °C—1 h) and 41 $\mu\Omega$ cm (350 °C—3 h). The negative TCR for the AD and low temperature annealed films is clearly due to their amorphous nature, with the AD film being completely amorphous while the 200 °C annealed films consist of fcc Cu-rich nanocrystals embedded in a continuous

amorphous matrix. Amorphous metals and alloys often exhibit a negative TCR, especially if $\rho_{300\,\mathrm{K}} > 150\ \mu\Omega$ cm, as per the Mooij criterion [14]. In the present case, the values of $\rho_{300\,\mathrm{K}}$ are somewhat less than the Mooij limit but still lead to the marginally negative TCR values, and the electron scattering mechanisms are presumably similar to those observed in other amorphous metals and alloys [15, 16]. Annealing at 350 °C leads to complete crystallization and results in a positive TCR, as expected for a crystalline metallic conductor.

All the five films studied show a sharp decrease in ρ at low temperatures, signaling the onset of a superconducting transition. Figures 4(b) and (c) show the low temperature resistivity normalized to the value at 7 K, amplified to highlight the onset and zero-resistance behaviors, respectively. The AD film exhibits a relatively sharp reduction in the normalized resistance ratio at ∼3.7 K (figure 4(b)) but it plateaus out at ∼0.85 and does not approach zero. Thus, the AD film either does not become truly superconducting or undergoes a second (unobserved) transition below 3 K. The low value of the $(T_C)_{\mathrm{onset}}$ observed in the amorphous system compared to bulk crystalline Nb ($T_C = 9.2$ K) is consistent with previous reports of Nb-based amorphous alloy systems [17]. This is attributed to changes in the phonon spectrum and electronic density of states in amorphous, 4d transition elements.

Interestingly, the drops in $R(T)/R(7\ \mathrm{K})$ below 7 K in the case of the 200 °C annealed samples, are not abrupt but appear to be spread over a temperature range with $(T_C)_{\mathrm{onset}} \approx 5.7$ K, before dropping sharply to values close to zero below ≈3.7 K. The difference in the superconducting behavior of the AD and 200 °C annealed films can be understood on the basis of their microstructural features. In the completely amorphous, phase-separated Cu–Nb film (AD), the 2–3 nm sized Nb-rich regions probably undergo a superconducting transition with $(T_C)_{\mathrm{onset}} \approx 3.7$ K, but these regions are largely isolated, and there is no continuous conducting path connecting the superconducting regions. Consequently, the AD film exhibits a relatively large residual resistivity at low temperatures, below the drop at 3.7 K. However, the formation of fcc Cu-rich nanocrystals in the 200 °C annealed films, leads to local Nb enrichment in the adjoining retained amorphous matrix. While the pre-existing Nb-rich, amorphous regions presumably still have the same composition with $(T_C)_{\mathrm{onset}} \approx 3.7$ K, the amorphous, Nb-rich regions in the vicinity of the fcc nanocrystals presumably exhibit a higher T_C due to an even higher Nb content. Consequently, the drops in $R(T)/R(7\ \mathrm{K})$ occur in multiple steps with a higher $(T_C)_{\mathrm{onset}} \approx 5.7$ K. Finally the entire film exhibits a superconducting-like behavior, which is clearly ascribable to these Nb-rich regions.

In contrast, both the Cu–Nb films annealed at 350 °C exhibit a rather sharp drop in $R(T)/R(7\ \mathrm{K})$ with $(T_C)_{\mathrm{onset}} \approx 5.1$ K, and superconduct with $(T_C)_0 \approx 5$ K (figure 4(b)). Here, $(T_C)_0$ refers to the temperature below which the resistance is less than 1% of the resistance at 7 K. Note that below ≈5 K, the resistance does not plateau off but has a small, continuous slope where the resistance changes by ≈0.05%. This can be understood if we take the contributions to resistivity from the Cu crystallites which are not superconducting. A parallel resistor model between Nb and Cu crystallites would explain the existence of this slope. The almost completely crystalline nature of these films, consisting of a relatively homogeneous distribution of fcc Cu nanocrystals embedded in coarser bcc Nb grains, is presumably responsible for the sharp T_C. However, we point out that though this film consists of the bcc Nb phase, the T_C (≈5 K) is substantially lower than that of bulk, elemental Nb (9.2 K). Since these samples are almost completely crystalline, the large depression in T_C may be expected to arise either from finite size effects or from proximity effects. It has been recently established that in pure, nanocrystalline Nb (where the Nb crystallites are mutually separated by partially insulating, oxide-rich grain boundaries), the T_C shows a gradual suppression between 20 and 8 nm, below which size the system completely loses superconductivity [18]. However, in the case of the Cu–Nb samples annealed at 350 °C, the microstructure consists of rather large (≈100 nm) Nb-rich particles, in which are embedded many small Cu-rich nanocrystals. For such a microstructure, we may expect the superconducting properties to be controlled mainly by proximity effects arising from the presence of the nano-dispersed Cu phase. In section 4, we provide a quantitative estimate of the contribution of the proximity effect to such a situation.

4. Discussions

According to the superconducting proximity effect (SPE), the T_C of a normal metal (N) in proximity with a superconductor (S) gets modified if their dimensions are less than their respective coherence length $\xi_{N,S} = [\hbar D_{N,S}/2\pi k_B T]^{1/2}$, where D_N (D_S) is the diffusivity of the normal (superconducting) layer. The theory has been experimentally verified in bilayers and alternating multilayers of superconductors and normal metals [19, 20]. Further, it has recently been shown that one may apply the de Gennes–Werthamer SPE theory to a random distribution of superconductor and normal nanoparticles (with grain sizes smaller than their respective coherence lengths), by replacing the ratio of the thicknesses of the superconductor and normal layers (d_S/d_N) by the ratio of their volume fraction [21, 22]. The micrographs of the films annealed at 350 °C (figure 3) show uniform fcc Cu nanocrystals (with mean size ≈18 ± 2 nm), separated by bcc Nb-rich regions, with a mean width of 12.5 ± 1.5 nm. As these dimensions are much lower than the coherence length of Nb (38 nm [23]), we can model the system as alternating layers of Cu and Nb with $d_N \approx 18$ nm and $d_S \approx 12$ nm. The T_C of the composite system is then given by [19]:

$$T_{cNS} = \frac{\Theta_D}{1.45} \exp\left[-\frac{1}{[N(0)V]_{\mathrm{eff}}}\right] \qquad \text{where}$$

$$[N(0)V]_{\mathrm{eff}} = \frac{N_S^2 V_S d_S + N_N^2 V_N d_N}{N_S d_S + N_N d_N}.$$

Here, N_S (N_N) is the DOS of the superconductor (normal metal) at the Fermi level, Θ_D is the Debye temperature and V is the electron–phonon interaction potential. The T_C was calculated using the following parameters from the literature: $N_N = 0.141N_0$ [21], $N_S = 0.94N_0$ [24], $V_S = 0.283/N_0$, $V_N = 0$ (N_0 = Avogadro number). Here, V_S was obtained

from the formula for T_C in the weak coupling limit. The Θ_D was taken as a weighted (as per the measured atomic ratio) mean of the Debye temperatures of Cu and Nb. The T_C obtained from this calculation (with no other free parameter) is 4.93 K, which is in excellent agreement with our measured value of $(T_C)_0 \approx 5$ K. The depression in the T_C in the phase-separated Cu–Nb sample annealed at 350 °C can thus be satisfactorily explained in terms of the proximity effect. It is significant that the superconducting proximity effect theory, which has been almost exclusively developed for and applied to bilayer and multilayer systems, can also be usefully applied to nanoscale phase-separated systems, using a simple logical extension of the theory.

In summary, we show that devitrification of the amorphous, nanoscale (≈2–3 nm) phase-separated, Cu–Nb system proceeds in two distinct steps. A nanocrystalline (≈10 nm) fcc copper-rich phase nucleates at lower temperatures, while a bcc niobium-rich phase nucleates at higher temperatures and engulfs the Cu-rich nanoparticles. The electrical resistivity measurements appear to be consistent with the observed microstructural evolution, Our study also provides an indication of the nature of superconductivity in amorphous Nb and highlights the role of the proximity effect in such phase-separated systems.

References

[1] Ma E 2005 *Prog. Mater. Sci.* **50** 413
[2] He J H, Sheng H W, Schilling P J, Chien C-L and Ma E 2001 *Phys. Rev. Lett.* **86** 2826
[3] He J H, Sheng H W and Ma E 2001 *Appl. Phys. Lett.* **78** 1343
[4] Michaelson C, Gente C and Bormann R 1997 *J. Appl. Phys.* **81** 6024
[5] Ma E 2003 *Scr. Mater.* **49** 941
[6] Duwez P, Willens R H and Clement W 1960 *J. Appl. Phys.* **31** 1136
[7] Linde R K 1966 *J. Appl. Phys.* **37** 934
[8] Hauser J J 1975 *Phys. Rev.* B **12** 5160
[9] Childress J R and Chien C L 1991 *Phys. Rev.* B **43** 8089
[10] Nastasi M, Saris F W, Hung L S and Mayer J W 1985 *J. Appl. Phys.* **58** 3052
[11] Banerjee R, Puthucode A, Bose S and Ayyub P 2007 *Appl. Phys. Lett.* **90** 021904
[12] Banerjee R, Bose S, Genc A and Ayyub P 2008 *J. Appl. Phys.* **103** 033511
[13] Puthucode A, Kaufman M J and Banerjee R 2008 *Metall. Mater. Trans.* A **39** 1578
[14] Mooij J H 1973 *Phys. Status Solidi* a **17** 521
[15] Naugle D G 1984 *J. Phys. Chem. Solids* **45** 367
[16] Lin J J and Wu C Y 1993 *Phys. Rev.* B **48** 5021
[17] Kerker G and Bennemann K H 1973 *Z. Phys.* **264** 15
Colver M M and Hammond R H 1973 *Phys. Rev. Lett.* **30** 92
[18] Bose S, Raychaudhuri P, Banerjee R, Vasa P and Ayyub P 2005 *Phys. Rev. Lett.* **95** 147003
[19] De Gennes P G 1964 *Rev. Mod. Phys.* **36** 225
[20] Hauser J J, Theurer H C and Werthamer N 1966 *Phys. Rev.* **142** 118
[21] Sternfeld I, Shelukhin V, Tsukernik A, Karpovski M, Gerber A and Palevski A 2005 *Phys. Rev.* B **71** 064515
[22] Bose S and Ayyub P 2007 *Phys. Rev.* B **76** 144510
[23] Cyrot M and Pavuna D 1992 *Introduction to Superconductivity and High-T_C Materials* (Singapore: World Scientific) p 38
[24] McMillan W L 1968 *Phys. Rev.* **167** 331